

Turnkey locking of quantum-dot lasers directly grown on Si

Received: 13 June 2023

Accepted: 26 February 2024

Published online: 26 April 2024

 Check for updates

Bozhang Dong^{1,6}, Yating Wan^{2,6}✉, Weng W. Chow³, Chen Shang¹, Artem Prokoshin², Emad Alkhazraji², Rosalyn Kosciwa⁴, Heming Wang¹ & John E. Bowers^{4,5}✉

Ultralow-noise laser sources are crucial for a variety of applications, including microwave synthesizers, optical gyroscopes and the manipulation of quantum systems. Silicon photonics has emerged as a promising solution for high-coherence applications due to its ability to reduce the system size, weight, power consumption and cost. Semiconductor lasers based on self-injection locking have achieved fibre laser coherence, but typically require a high-quality-factor external cavity to suppress coherence collapse through frequency-selective feedback. Lasers based on external-cavity locking are a low-cost and turnkey operation option, but their coherence is generally inferior to self-injection locking lasers. In this work, we demonstrate quantum-dot lasers grown directly on Si that achieve self-injection-locking laser coherence under turnkey external-cavity locking. The high-performance quantum-dot laser offers a scalable and low-cost heteroepitaxial integration platform. Moreover, the chaos-free nature of the quantum-dot laser enables a 16 Hz Lorentzian linewidth under external-cavity locking using a low-quality-factor external cavity, and improves the frequency noise by an additional order of magnitude compared with conventional quantum-well lasers.

Narrow-linewidth and frequency-stable lasers have opened up new opportunities for optical sensing and signal generation applications, including optical frequency and microwave synthesis^{1,2}, laser gyroscopes^{3,4}, light detection and ranging (LIDAR) systems⁵⁻⁷, spectroscopy⁸ and coherent optical communications⁹. In the quest for compact and mass-manufacturable coherent systems, photonic integrated circuits (PICs) have emerged as the most compelling solution. Semiconductor lasers with high-performance characteristics are integral components in the operation of PICs. Nevertheless, the linewidth of conventional semiconductor lasers ranges from hundreds of kilohertz to a few megahertz, which is more than seven orders of magnitude higher than the state-of-the-art bulk fibre lasers¹⁰. The inferior noise characteristics of semiconductor lasers have prevented their widespread utilization

in the aforementioned applications. Self-injection locking (SIL) and Pound–Drever–Hall locking technologies¹¹⁻¹⁶ have dramatically reduced the frequency noise and laser linewidth of semiconductor lasers. SIL, a passive locking technique, employs resonant optical feedback from a high-quality-factor (high-*Q*) external optical element to suppress the coherence collapse of the pump laser and enable the reduction of the laser linewidth below that of a fibre laser¹⁷. However, the SIL operation also requires that the pump laser frequency coincides with the external cavity resonance, introducing complexity and causing power penalties. These limitations need to be addressed to make this solution accessible to the industry.

In this work, we introduce advanced quantum-dot (QD) lasers as a compelling solution for high-coherence turnkey external-cavity-locking

¹Institute for Energy Efficiency, University of California, Santa Barbara, Santa Barbara, CA, USA. ²Integrated Photonics Laboratory, King Abdullah University of Science and Technology, Thuwal, Saudi Arabia. ³Sandia National Laboratories, Albuquerque, NM, USA. ⁴Materials Department, University of California, Santa Barbara, Santa Barbara, CA, USA. ⁵Department of Electrical and Computer Engineering, University of California, Santa Barbara, Santa Barbara, CA, USA. ⁶These authors contributed equally: Bozhang Dong, Yating Wan. ✉e-mail: yating.wan@kaust.edu.sa; bowers@ece.ucsb.edu

(ECL) technology. Semiconductor QDs, due to the atom-like density of states, exhibit near-zero linewidth enhancement factor (LEF) and thus remarkable frequency noise and linewidth¹⁸. Furthermore, QD lasers offer higher immunity to the non-radiative defects between the III–V elements and Si, making them suitable for monolithic integration on Si substrates, particularly with high-Q SiN microresonators^{19,20}. This integration approach is more cost-effective compared with the heterogeneous integration approach, eliminating the need for expensive III–V wafers^{21,22}. The chaos-free feature of QDs reduces the dependence for linewidth reduction on a high-Q microresonator, distinguishing QD lasers from conventional quantum-well (QW) lasers²³. By leveraging the high-performance QD laser, we achieved a 16 Hz Lorentzian linewidth—the smallest number ever achieved in on-chip QD lasers (to the best of our knowledge). Four orders of magnitude reduction in frequency noise has been achieved using a low-Q external cavity without a frequency filter. On the contrary, a QW laser, which is susceptible to coherence collapse under weak external feedback, requires a much larger external-cavity Q-factor to maintain coherence. Leveraging the high-feedback insensitivity of QD lasers, we improve the coherent feedback strength in the ECL operation, which allows for an extra one order of magnitude reduction in the frequency noise compared with its QW counterpart. In particular, our low-Q approach allows for turnkey locking without any power penalty, distinguishing it from the SIL approach that relies on a high-Q external cavity. Additionally, this approach offers greater flexibility for material platforms in which fabricating an ultrahigh-Q resonator is challenging. This work effectively addresses the limitations of SIL technology and contributes to enhancing the size, weight, power consumption and cost (SWaP-C) metrics of high-coherence PICs. In addition, our theoretical investigations indicate that the full potential of the QD laser has yet to be realized. By integrating them with complementary metal–oxide–semiconductor (CMOS)-ready high-Q microresonators, it becomes feasible to further reduce the linewidth to the sub-hertz level. These advancements position QD lasers as a compelling candidate for various high-coherence applications, including optical-frequency synthesizers, dual-comb spectroscopy and ultrahigh-capacity optical transceivers.

Results

Epitaxial growth of QD distributed-feedback lasers on Si

The QD-on-Si laser material was grown in a Veeco Gen-II solid-source molecular-beam-epitaxy chamber on an anti-phase domain-free GaP/Si on-axis template. After completing the defect-reducing buffer layers and the QD active region²⁴, the sample is removed from the chamber for grating patterning. Supplementary Fig. 1 shows the atomic force microscopy scan of the exposed surface dots and the photoluminescence spectrum of the whole active region. A uniform first-order distributed-feedback (DFB) grating, with a duty cycle of 50%, an etch depth of 50 nm and a period of 197 nm, was dry etched into the top GaAs layer by inductively coupled plasma with Cl₂/N₂-based chemistry. An electron-beam-lithography-patterned SiO₂ hard mask was used to transfer the pattern. Before the sample was loaded back into the chamber for the regrowth of the top cladding and contact layers, a rigorous surface treatment combining solvent clean, O₂ plasma ash and HF dip was performed. Thereafter, an in situ atomic H clean for 30 min at 450 °C was conducted to remove any native oxide. The second molecular-beam-epitaxy growth then proceeded with a 2 nm p-GaAs nucleation layer and the rest of a standard GaAs/Al_xGa_{1-x}As graded-index separate confinement heterostructure. Supplementary Fig. 2 provides details about the processing flow. The as-grown material was then processed into deeply etched waveguides, with ridge widths ranging from 1.7 to 3.0 μm. The scanning transmission electron microscopy image and the epi-structure of the QD laser are shown in Fig. 1a. Supplementary Table 1 provides details about the height of each epilayer. The QD chipset is then mounted into a butterfly package (Fig. 1b) to facilitate measurements and enable portability.

High-performance integrated QD lasers

Owing to the quantized density of states, the carriers are tightly confined in the dots, leading to enhanced injection efficiency²⁵. From a series of devices measured, a maximum power of 11.7 mW is obtained from a 5 × 1,500 μm² cavity, twice the previously reported value²⁶. The lowest threshold current of 10 mA is achieved from a 2.5 × 800.0 μm² cavity. The lowest threshold current density of 400 A cm⁻² is obtained from a 2 × 1,500 μm² cavity, which corresponds to 80 A cm⁻² per QD layer. At room temperature (20 °C), the QD laser exhibits a stable single-mode emission in the presence of a side-mode-suppression ratio (SMSR) above 50 dB above the threshold (Fig. 1e). An SMSR value of 59 dB is achieved when the laser operates at 35 mA. The current coefficient of the Bragg wavelength is as low as 0.022 nm mA⁻¹ (Fig. 1d). It should be noted that the threshold current of a DFB laser is not only determined by the gain medium but also depends on the optical mismatch between the laser gain peak and the Bragg wavelength²⁷. Such an optical mismatch can be detuned by varying the operating temperature due to the different temperature coefficients of gain and DFB wavelengths. Figure 1c depicts the evolution of the Bragg wavelength caused by the temperature variation. The extracted temperature coefficient of 0.077 nm °C⁻¹ is much lower than the temperature coefficient of the optical gain peak. As a result of the reduction in optical mismatch, the threshold current is reduced from 15 to 13 mA as the temperature increases from 20 to 35 °C (Fig. 1f). On the other hand, it should be noted that the requirement of laser cooling is a major challenge for PICs due to laser degradation at elevated temperatures. Such an inconvenience comes from both increased non-radiative carrier recombination and reduced gain due to the wider spreading of the Fermi distribution of carriers when they are heated up. Three-dimensional carrier confinement in III–V QDs equips these nanoparticles with superior insensitivity to growth defects for the largely reduced carrier diffusion length compared with QWs²⁸. The large energy separation between the ground and excited states from the tight carrier confinement also enables better thermal stability²⁴. A QD laser with a 1-mm-long cavity yields a characteristic temperature T_0 of 113 K in the range of 35–55 °C, and T_0 of 40 K in the range of 55–80 °C. A moderate cavity length of 1.5 mm allows for improving T_0 to 423 and 92 K in the range of 35–55 °C and 55–80 °C, respectively (Fig. 1f). It should be noted that T_0 extracted in the elevated-temperature range is underestimated due to the additional increase in the threshold current induced by the aforementioned optical mismatch. In addition to the lasing performance, the QD laser is also beneficial to coherent applications owing to its near-zero LEF¹⁸. It is worth stressing that the QD laser does not suffer from any degradation in the LEF when it is directly grown on Si. In the case of a single-frequency DFB laser, it is crucial to reduce the optical mismatch to take advantage of the intrinsic LEF of the active region. Figure 1g depicts the frequency-noise spectra of the QD DFB laser with a cavity length of 1.0 mm (burgundy) and 1.5 mm (navy blue). The fibre-coupled power is fixed to 0 dBm and both devices operate at room temperature where the optical mismatch approaches zero. Both devices exhibit remarkable frequency noise in the presence of a white-noise level below 1.8 × 10⁴ Hz² Hz⁻¹. A slightly better linewidth is observed in the 1.5-mm-long QD laser, where the white-noise level is as low as 1.3 × 10⁴ Hz² Hz⁻¹, yielding a Lorentzian linewidth of 41 kHz.

Chaos-free operation under EOF

Laser dynamics under external optical feedback (EOF) have been extensively studied during the past four decades. The stability and instability of semiconductor lasers under EOF have opened up various applications. Coherent feedback allows for an increase in the intracavity photon density, which is beneficial to largely reduce the laser linewidth. Nevertheless, a strong EOF would possibly lead to a severe coherence collapse. To take advantage of the narrow linewidth under EOF, it is crucial to suppress the coherence collapse of the laser. Compared with the conventional QW laser, the chaos-free QD laser

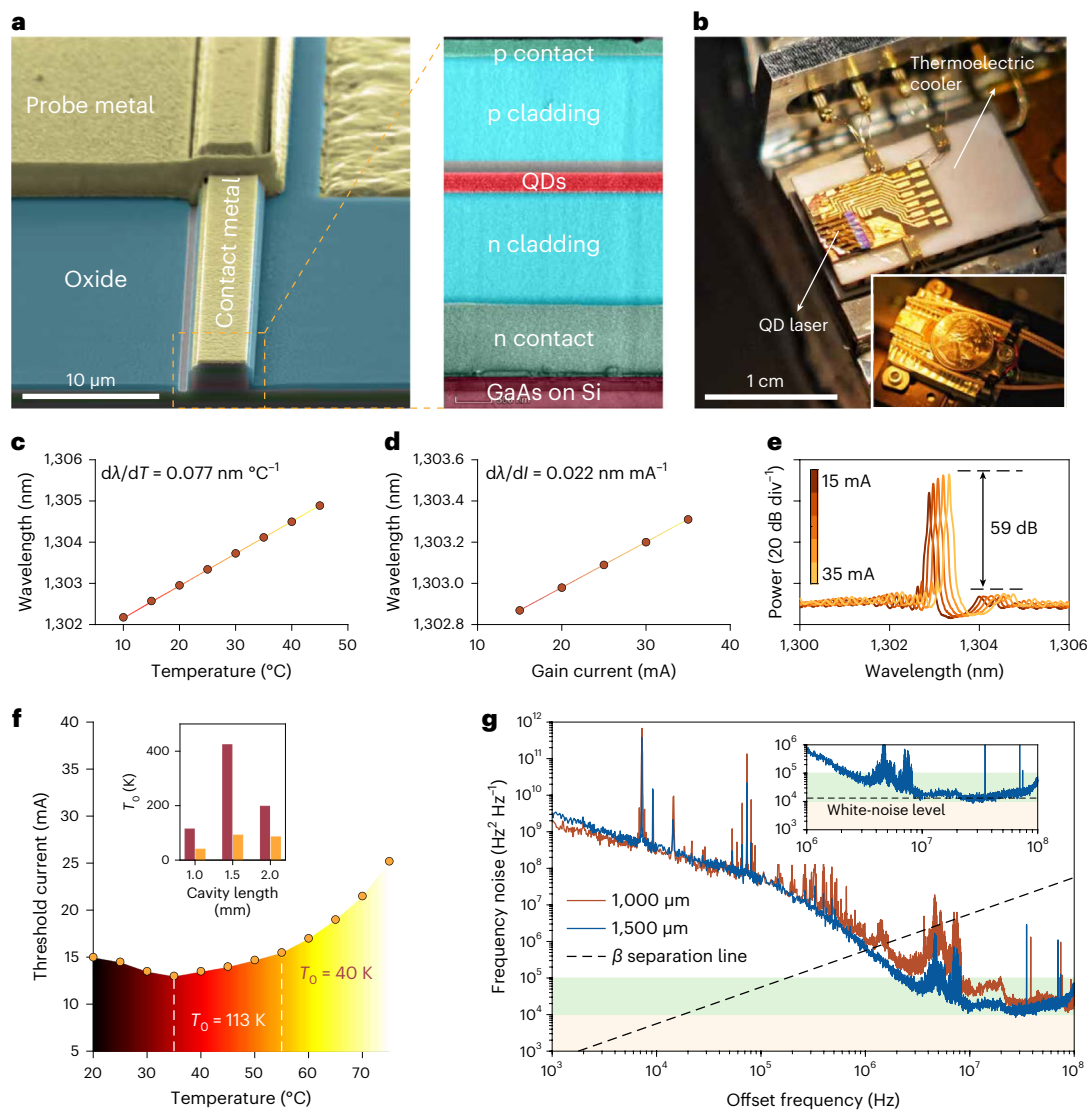


Fig. 1 QD laser design and characterizations. **a**, Cross-sectional view of the (001)-axis bright-field scanning transmission electron microscopy image. **b**, Images of the QD laser in a compact butterfly package. **c**, DFB wavelength as a function of operating temperature in a device with a $3 \times 1,000 \mu\text{m}^2$ cavity. **d**, DFB wavelength as a function of gain current. **e**, Evolution of the optical spectra by increasing the injection current from the threshold current in a device with a $3 \times 1,000 \mu\text{m}^2$ cavity. The optimum SMSR is 59 dB. The threshold

current at room temperature (20°C) is 15 mA. **f**, Threshold current as a function of operating temperature. The inset shows the characteristic temperature T_0 , in the ranges of 35–55 and 55–80 °C with different cavity lengths. $T_0 = 423\text{ K}$ within 35–55 °C for the device with 1.5 mm cavity length. **g**, Frequency-noise spectra of the 1.0 mm device (burgundy) and another 1.5-mm-long QD laser (navy blue). The output power is fixed at 0 dBm. The inset shows a zoomed-in view on the white-noise level. The free-running QD laser yields a Lorentzian linewidth of 41 kHz.

opens up new opportunities for high-coherence PICs²⁹. Figure 2d depicts the laser linewidth as a function of the on-chip feedback strength for a wavelength-detuned QD laser as its output power is fixed at 0 dBm. The experimental setup for the EOF and linewidth characterization are shown in Fig. 2a. The QD laser remains in regime I in which the linewidth is unaffected when the feedback strength is below –35 dB. As the on-chip feedback strength increases from –35.0 to –9.6 dB, which is achievable by taking advantage of the low-loss SiN waveguide, a notable linewidth reduction takes place and the QD laser enters into regime II. On a periodic modulation of the feedback strength between –60.0 and –9.6 dB, the QD laser exhibits a turnkey transition from the unlocked state to the locked state, and vice versa (Fig. 2e). On the contrary, the QW laser is much more sensitive to the EOF than the QD laser. Figure 2g depicts the evolution of laser linewidth due to external feedback for a commercial QW laser. The output power of the QW laser is fixed at 0 dBm for a fair comparison. Despite the ECL regime (regime II) when the feedback strength is in the range of –70 and –37 dB, the QW laser suffers

from coherence collapse (regime IV) when the feedback strength is above –37 dB. A zoomed-in view of the transition from regime II to regime IV is shown in Fig. 2h.

The 35 dB improved feedback insensitivity in the wavelength-detuned QD laser is mainly attributed to the large damping factor³⁰. Supplementary Section IV provides detailed discussions on feedback insensitivity. Despite the fact that a near-zero LEF is beneficial for suppressing the coherence collapse, it is not always favourable to the ECL since it suppresses regime II, too²⁷. On the other hand, a large LEF is crucial to realize a notable linewidth narrowing³¹. To suppress the coherence collapse and achieve large linewidth narrowing, we propose increasing the optical mismatch between the optical gain peak and Bragg wavelength in the QD laser. In this study, we employ a well-designed DFB grating to enable the laser to operate at 1,323 nm, which is 12 nm away from the gain peak at room temperature. As a result, the LEF of the lasing mode at the threshold is increased to 2.6, comparable with that of the QW lasers. Supplementary Fig. 4 shows the

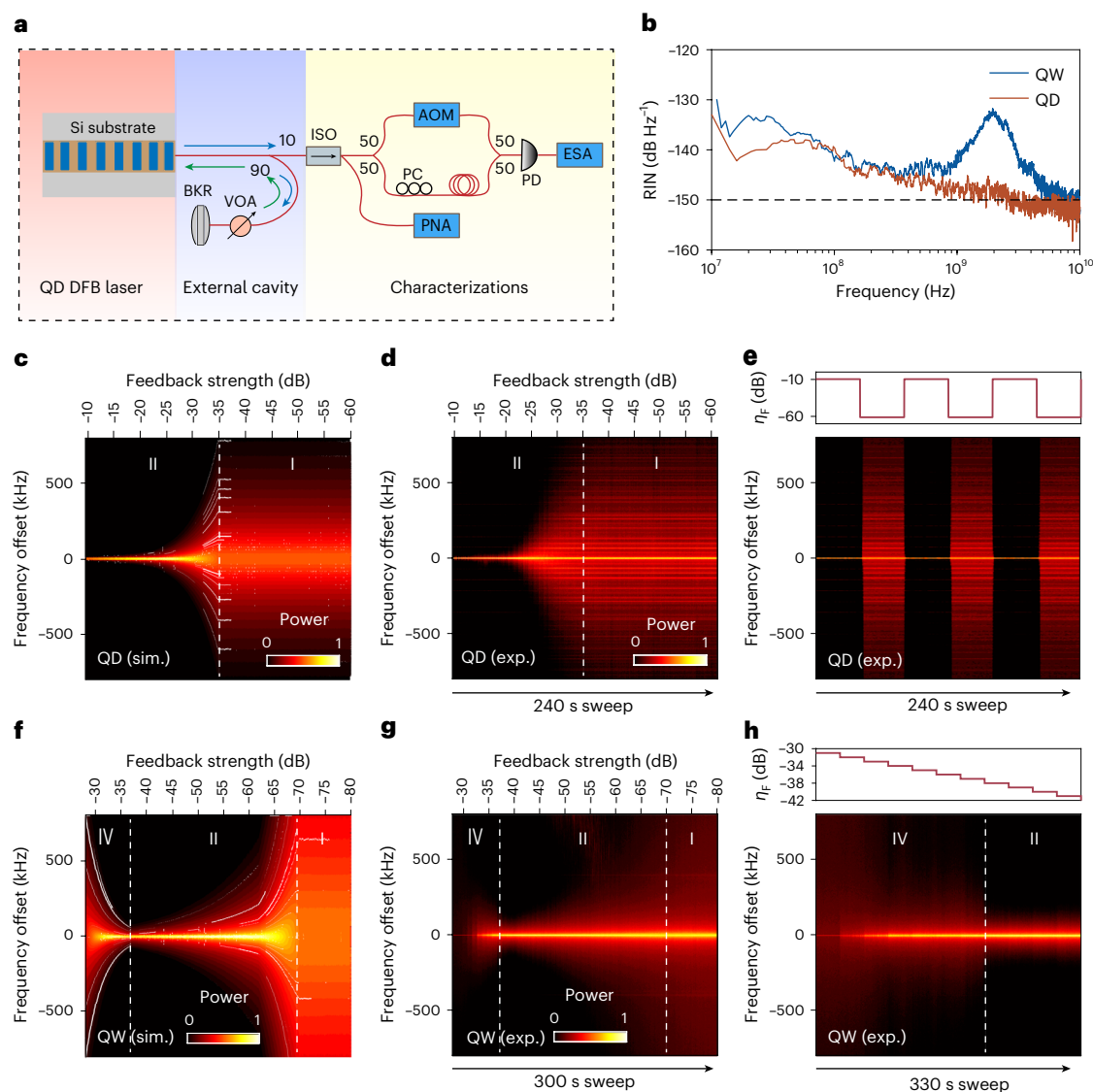


Fig. 2 | Laser dynamics under EOF. **a**, Experimental setup for the ECL, including an off-chip external cavity and a self-heterodyne setup for linewidth characterizations. VOA, variable optical attenuator; BKR, back-reflector; ISO, optical isolator; PC, polarization controller; AOM, acousto-optic modulator; PD, photodiode; ESA, electrical spectrum analyser; PNA, phase-noise analyser. **b**, RIN of the free-running QD (burgundy) and QW (navy blue) laser. The output power of both lasers is fixed at 0 dBm. **c**, Theoretically calculated mapping of the spectral linewidth as a function of the feedback strength of the QD laser.

d, Experimentally measured mapping of the spectral linewidth as a function of the feedback strength of the QD laser. **e**, Turnkey operation of the ECL QD laser under a modulation of the feedback strength between -60.0 and -9.6 dB. **f**, Theoretically calculated mapping of the spectral linewidth as a function of the feedback strength of the QW laser. **g**, Experimentally measured mapping of the spectral linewidth as a function of the feedback strength of the QW laser. **h**, Transition from regime II to regime IV of the QW laser. Regime I, stable-operation regime; regime II, ECL regime; regime IV, coherence-collapse regime.

optical spectrum of this wavelength-detuned QD laser as well as the extraction of the LEF. The consequent increase in internal loss results in an increase in the threshold current to 60 mA (Fig. 3c). Despite the increased LEF, the strong damping of the QD laser can still suppress the coherence collapse. Supplementary Section IV provides the theoretical analyses of the difference in feedback sensitivity between the QD and QW lasers. The simulation results are summarized in Fig. 2c,f, which are in good agreement with the experiments. Here, through theory, we have validated that a design of the optical mismatch in a QD DFB laser enables a linewidth-reduction regime and maintains laser coherence. Moreover, the strong damping of the QD laser is advantageous for suppressing the relaxation oscillation frequency, resulting in lower relative intensity noise (RIN). Figure 2b depicts the RIN spectra of the free-running QD (burgundy) and QW (navy) lasers at an output power of 0 dBm. The RIN value of the QD laser is lower

than that of the QW counterpart in the frequency range from 10 MHz to 10 GHz, which is promising for LIDAR applications. Supplementary Section III discusses more details about the measurements of the damping factor.

Turnkey locking without power penalty

The severe coherence collapse in a conventional QW laser can be suppressed through the use of a high- Q external cavity that offers frequency-selective feedback (Fig. 3b). This approach provides a narrow-frequency filter that only allows the coherent photons to go back to the laser cavity, thus suppressing the coherence collapse of the laser and enabling the QW laser to achieve large linewidth narrowing through the strong backscattering of the microresonator. Nevertheless, this approach requires a high- Q resonator, which can be a challenge to fabricate. Any degradation in the Q -factor of the external cavity due to

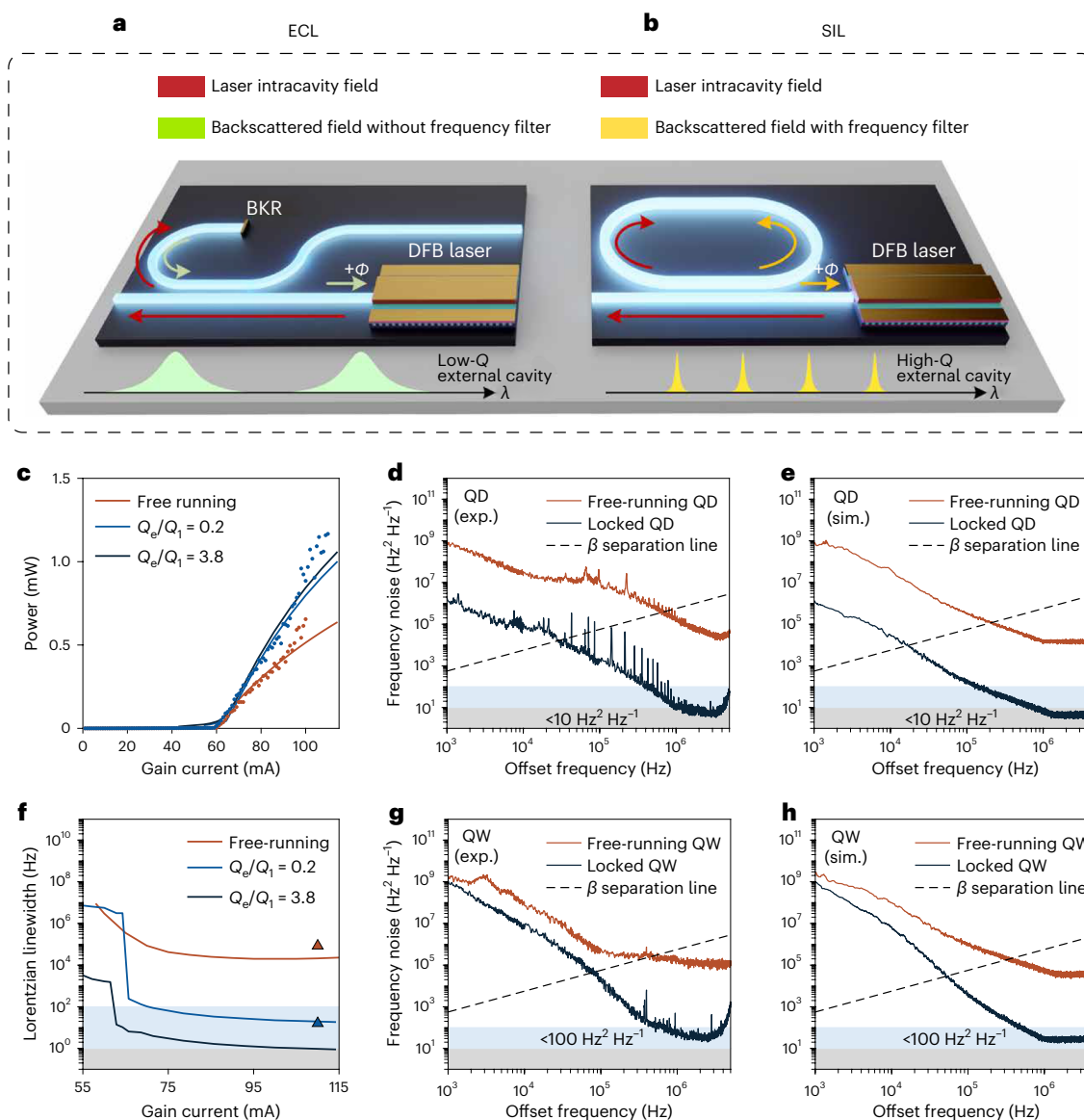


Fig. 3 | Turnkey ECL operation. **a**, Operation of turnkey ECL by using a low- Q external cavity. A back-reflector is used to reflect the laser emission (red arrow) back to the laser cavity. The laser operating in feedback regime II allows the delayed laser field (green arrow) to go back to the laser cavity and interact with the intracavity field for linewidth reduction. In this work, the external cavity is developed by using an optical fibre and a fibre-based reflector. **b**, Operation of SIL by using a high- Q microresonator. A high- Q external cavity provides a narrow-frequency filter for the pump laser, which enables frequency-selective external feedback. The pump laser light (red arrow) should be controlled to anchor to one of the external cavity resonances to generate a reflected field. The backscattered coherent light (yellow arrow) is reinjected into the laser cavity and interacts with the intracavity field for linewidth reduction. **c**, Calculated light–current characteristics (LI; solid curves) of the wavelength-detuned QD laser in free-running (burgundy) and ECL operations.

In both low- Q (navy blue) and high- Q (black) locking conditions, the QD laser does not suffer from a power penalty. The measured LIs are shown by the coloured bullet points. **d**, Frequency-noise spectra of the QD laser in free-running (burgundy) and ECL (black) operations in the experiment. **e**, Calculated frequency-noise spectra of the QD laser in free-running (burgundy) and ECL (black) operations. **f**, Calculated Lorentzian linewidth as a function of injection current in free-running (burgundy) and ECL operations. A low- Q locking condition (navy blue) in this work allows for a 16 Hz linewidth. A high- Q condition (black) can further reduce the laser linewidth to the hertz level. Experimental results are shown by the coloured-triangle symbols. **g**, Frequency-noise spectra of the QW laser in free-running (burgundy) and ECL (black) operations in the experiment. **h**, Calculated frequency-noise spectra of the QW laser in free-running (burgundy) and ECL (black) operations.

fabrication issues can lead to a worsening of laser linewidth locking or even a failure of the SIL. Moreover, anchoring the laser frequency to one of the external cavity resonances demands careful setpoints for laser linewidth locking; the laser also suffers from a power penalty due to the limitation of the Q -factor of the external cavity. On the contrary, a low- Q external cavity provides a turnkey option for laser linewidth reduction without causing any power penalty (Fig. 3a). Nevertheless, the laser can suffer from coherence collapse under strong feedback without a frequency filter.

It used to be a challenge to reduce the QW laser linewidth to the hertz level with a low- Q external cavity, due to the weak coherent feedback that it offers. In general, the coherence of QW external-cavity lasers is more than one order of magnitude inferior to the high- Q SIL lasers^{32–34}. Such a performance gap is attributed to the coherence collapse of the QW laser under strong external feedback. Using the ECL approach by applying the maximum coherent feedback strength of -39.0 dB, the QW laser linewidth is reduced to 111 Hz, which is 34.9 dB lower than its free-running linewidth (Fig. 3g). On the contrary, the

Table 1 | Performance comparison of narrow-linewidth lasers using high-Q SIL and low-Q ECL approaches

| Operation principle | Configuration (G/EC) | Q (M) | Linewidth (Hz) | Reference |
|---------------------|---|-------|----------------|-----------|
| ECL | Monolithic QD-Si/optical fibre | N/A | 16 | This work |
| SIL | Hybrid III-V/Si ₃ N ₄ | 164 | 0.04 | 17 |
| SIL | Hybrid III-V/Si ₃ N ₄ | 260 | 1.2 | 14 |
| SIL | Heterogeneous III-V/Si ₃ N ₄ | 50 | 5 | 38 |
| SIL | Heterogeneous III-V/Si ₃ N ₄ | 7 | 25 | 39 |
| SIL | Hybrid III-V/Si ₃ N ₄ | >15 | 25 | 7 |
| SIL | Heterogeneous III-V/Si ₃ N ₄ | 10 | 92.4 | 40 |
| SIL | Hybrid III-V/Si ₃ N ₄ -LiNbO ₃ | 1.9 | 3,140 | 42 |
| ECL | Hybrid III-V/Si ₃ N ₄ | N/A | 40 | 48 |
| ECL | Heterogeneous III-V/Si ₃ N ₄ | N/A | 140 | 32 |
| ECL | Heterogeneous III-V/Si ₃ N ₄ | N/A | 400 | 49 |
| ECL | Monolithic III-V | N/A | 50,000 | 50 |

G, gain medium; EC, external cavity.

chaos-free QD laser allows for bridging the gap between the ECL and SIL approaches. In this study, the low-*Q* external cavity is developed by using an optical fibre and a fibre-based reflector without frequency filtering. With both lasers having their output powers fixed at 0 dBm for a fair comparison, a 37.2 dB suppression of the white-noise level and a 16 Hz Lorentzian linewidth have been achieved by a QD laser under an on-chip resonant feedback strength of -9.6 dB (Fig. 3d). The frequency-noise reduction is greater than 30 dB across the entire offset frequency range from 1 kHz to 5 MHz. Such a record QD laser linewidth, requiring no sophisticated tuning and locking, is on par with the SIL QW lasers using a high-*Q* resonator. The turnkey locking of the QD laser exhibited long-term stability, in the presence of a repeatable narrow linewidth holding for at least 40 s (Fig. 2e). Moreover, in both experiment and theory, we demonstrate that the laser source does not suffer from a power penalty by using the ECL approach. On the contrary, the laser output power gets amplified in the locking operation owing to the additional coherent photons given by the reflected field for lasing (Fig. 3c).

The remarkable ECL performance of the QD laser is twofold. First, the QD laser allows for generating a narrower free-running linewidth than the QW laser owing to its lower LEF. The free-running linewidth of the wavelength-detuned QD laser is 84 kHz, which is four times narrower than its QW counterpart. Second, the chaos-free QD laser does not require a frequency filter to suppress the coherence collapse; thus, it can take advantage of the strong coherent feedback offered by a low-*Q* external cavity. As a result, both linewidth and linewidth reduction ratio are improved by utilizing the QD laser. Supplementary Section V provides the theoretical analyses of frequency-noise reduction. The calculated frequency noise of the QD and QW lasers are shown in Fig. 3e,h, respectively, which agree with the experiments. Last, it should be noted that the QD laser is also compatible with the high-*Q* SIL approach and its full potential has yet to be realized. In this work, the 16 Hz intrinsic linewidth is obtained by using an external cavity whose *Q*-factor is inferior to the *Q*-factor of the laser cavity ($Q_e/Q_l = 0.2$ in theory; Fig. 3f, blue curve). Our theory indicates that the laser linewidth can be further reduced to the hertz level by increasing the *Q*-factor of the external cavity beyond that of the laser cavity ($Q_e/Q_l = 3.8$ in theory; Fig. 3f, black curve).

Discussion and outlook

This work demonstrates a high-performance QD laser on Si that achieves a Lorentzian linewidth of 16 Hz under ECL. The quantized

QD laser opens up more opportunities for large-scale PICs owing to its compatibility with the mature CMOS foundry. Compared with QD lasers grown on the native substrate, directly growing the QD lasers on Si improves not only the scalability using commercial 300 mm Si wafers but also the laser performance. For instance, the epitaxial QD laser on Si enabled a record LEF as low as 0.13 (ref. 18), whereas the LEF reported in the native QD laser was, in general, above 0.70 (ref. 35). Such an improvement results from the optimization of the inhomogeneous broadening and defects. The shortening of the Shockley–Read–Hall recombination time also contributes to the near-zero LEF in the epitaxial QD laser on Si (ref. 36). Superior to the conventional QW heterostructure, the advanced QD enables the monolithic integration of laser sources, amplifiers and detectors on Si, which is a low-cost solution for Si PICs. After optimizing the fabrication process, the QD DFB laser performance has been improved. This includes a decrease in the threshold current density to 400 A cm^{-2} , an increase in SMSR to 59 dB, a reduction in the intrinsic linewidth to 41 kHz and an improvement in the yield²⁶. Previous studies have shown that the near-zero LEF offered by the QD laser allows for isolator-free photonic integration³⁷. Here we reveal that the LEF of the QD laser can be practically engineered by wavelength detuning between the optical gain peak and Bragg wavelength. As such, an increase in the LEF through a wavelength-detuned DFB grating contributes to a large linewidth reduction as the laser's coherence is maintained. By leveraging the chaos-free operation of the QD laser, its linewidth can be locked to a low-*Q* external cavity without the need for a frequency filter. Table 1 compares the current state-of-the-art narrow-linewidth lasers using either the high-*Q* SIL approach or the low-*Q* ECL approach. Although an ultrahigh-*Q* resonator using the low-loss SiN platform enables hertz- and sub-hertz-level laser linewidths^{14,17,38}, fabrication is challenging as any degradation in the *Q*-factor would result in a broader laser linewidth^{7,39,40}. In addition, achieving ultrahigh-*Q* resonators in many material platforms, such as lithium niobate⁴¹, poses major challenges. As a result, the locked linewidth of SIL lasers using lithium niobate resonators is on the order of kilohertz⁴², which remains to be improved for coherent LIDAR applications. Our work, however, demonstrates that the locked QD laser linewidth is on par with or even better than most high-*Q* SIL QW lasers. This finding underscores the potential of QD lasers in applications requiring precise coherence, particularly where achieving ultrahigh-*Q* resonators is challenging. In addition, our approach provides additional benefits including turnkey and power-maintaining operations. On the other hand, employing a low-*Q* external cavity can potentially enhance the operation stability due to its broader reflection bandwidth, which is more accommodating of shifts in laser wavelength. Along with the high thermal stability of epitaxial QD lasers on Si—capable of continuous-wave operation above 150 °C (ref. 43)—this approach is beneficial to the robustness of ECL in high-temperature operation.

Further improving the laser coherence can be effectively achieved with an on-chip external cavity solution. Using a fibre-based external cavity, the feedback strength is mainly limited by the laser-to-fibre coupling loss. By leveraging the laser and external cavity on the same chip, this coupling loss can be largely reduced. Three-dimensional photonic integration can potentially leverage the ultralow-loss SiN waveguide, which is advantageous for maximizing the on-chip coherent feedback strength and reducing the laser linewidth³⁸.

Another approach to improve the SIL is to apply a frequency filter by using a high-*Q* resonator. The QD laser is also compatible with the CMOS-ready SiN and silica microresonators that offer a *Q*-factor of one billion^{44,45}. We theoretically demonstrate that sub-hertz-level linewidth can be achieved by using a QD laser and a high-*Q* resonator^{46,47}. Additionally, spiral microresonators with large modal volumes can be employed to reduce the low-offset frequency noise caused by thermodynamic fluctuations¹⁷. Depending on the design of the external cavity, the high-coherence QD laser can scale up to 300 mm Si wafers using either monolithic or heterogeneous photonic integration

technologies. This would lead to low-cost, large-volume and scalable production. The potential for the monolithic integration of III–V lasers and passive waveguides onto a single chip using foundry-based technologies could further advance the development of QD lasers and their integration into practical photonic applications.

Online content

Any methods, additional references, Nature Portfolio reporting summaries, source data, extended data, supplementary information, acknowledgements, peer review information; details of author contributions and competing interests; and statements of data and code availability are available at <https://doi.org/10.1038/s41566-024-01413-2>.

References

1. Spencer, D. T. et al. An optical-frequency synthesizer using integrated photonics. *Nature* **557**, 81–85 (2018).
2. Marpaung, D., Yao, J. & Capmany, J. Integrated microwave photonics. *Nat. Photon.* **13**, 80–90 (2019).
3. Gundavarapu, S. et al. Sub-hertz fundamental linewidth photonic integrated Brillouin laser. *Nat. Photon.* **13**, 60–67 (2019).
4. Lai, Y.-H. et al. Earth rotation measured by a chip-scale ring laser gyroscope. *Nat. Photon.* **14**, 345–349 (2020).
5. Trocha, P. et al. Ultrafast optical ranging using microresonator soliton frequency combs. *Science* **359**, 887–891 (2018).
6. Suh, M.-G. & Vahala, K. J. Soliton microcomb range measurement. *Science* **359**, 884–887 (2018).
7. Lihachev, G. et al. Low-noise frequency-agile photonic integrated lasers for coherent ranging. *Nat. Commun.* **13**, 3522 (2022).
8. Suh, M.-G., Yang, Q.-F., Yang, K. Y., Yi, X. & Vahala, K. J. Microresonator soliton dual-comb spectroscopy. *Science* **354**, 600–603 (2016).
9. Olsson, S. L. et al. Probabilistically shaped PDM 4096-QAM transmission over up to 200 km of fiber using standard intradyne detection. *Opt. Express* **26**, 4522–4530 (2018).
10. Matei, D. et al. 1.5 μm lasers with sub-10 mHz linewidth. *Phys. Rev. Lett.* **118**, 263202 (2017).
11. Dahmani, B., Hollberg, L. & Drullinger, R. Frequency stabilization of semiconductor lasers by resonant optical feedback. *Opt. Lett.* **12**, 876–878 (1987).
12. Hollberg, L. & Ohtsu, M. Modulatable narrow-linewidth semiconductor lasers. *Appl. Phys. Lett.* **53**, 944–946 (1988).
13. Laurent, P., Clairon, A. & Breant, C. Frequency noise analysis of optically self-locked diode lasers. *IEEE J. Quantum Electron.* **25**, 1131–1142 (1989).
14. Jin, W. et al. Hertz-linewidth semiconductor lasers using CMOS-ready ultra-high-Q microresonators. *Nat. Photon.* **15**, 346–353 (2021).
15. Lihachev, G. et al. Platicon microcomb generation using laser self-injection locking. *Nat. Commun.* **13**, 1771 (2022).
16. Guo, J. et al. Chip-based laser with 1-hertz integrated linewidth. *Sci. Adv.* **8**, eabp9006 (2022).
17. Li, B. et al. Reaching fiber-laser coherence in integrated photonics. *Opt. Lett.* **46**, 5201–5204 (2021).
18. Duan, J. et al. Semiconductor quantum dot lasers epitaxially grown on silicon with low linewidth enhancement factor. *Appl. Phys. Lett.* **112**, 251111 (2018).
19. Liu, A. Y., Srinivasan, S., Norman, J., Gossard, A. C. & Bowers, J. E. Quantum dot lasers for silicon photonics. *Photonics Res.* **3**, B1–B9 (2015).
20. Shang, C. et al. Electrically pumped quantum-dot lasers grown on 300 mm patterned Si photonic wafers. *Light Sci. Appl.* **11**, 299 (2022).
21. Shang, C. et al. Perspectives on advances in quantum dot lasers and integration with Si photonic integrated circuits. *ACS Photonics* **8**, 2555–2566 (2021).
22. Zhou, Z. et al. Prospects and applications of on-chip lasers. *eLight* **3**, 1 (2023).
23. Dong, B. et al. Dynamic and nonlinear properties of epitaxial quantum-dot lasers on silicon operating under long- and short-cavity feedback conditions for photonic integrated circuits. *Phys. Rev. A* **103**, 033509 (2021).
24. Shang, C. et al. High-temperature reliable quantum-dot lasers on Si with misfit and threading dislocation filters. *Optica* **8**, 749–754 (2021).
25. Wan, Y. et al. High speed evanescent quantum-dot lasers on Si. *Laser Photonics Rev.* **15**, 2100057 (2021).
26. Wan, Y. et al. 1.3 μm quantum dot-distributed feedback lasers directly grown on (001) Si. *Laser Photonics Rev.* **14**, 2000037 (2020).
27. Dong, B. et al. Dynamic performance and reflection sensitivity of quantum dot distributed feedback lasers with large optical mismatch. *Photonics Res.* **9**, 1550–1558 (2021).
28. Selvidge, J. et al. Non-radiative recombination at dislocations in InAs quantum dots grown on silicon. *Appl. Phys. Lett.* **115**, 131102 (2019).
29. Grillot, F., Duan, J., Dong, B. & Huang, H. Uncovering recent progress in nanostructured light-emitters for information and communication technologies. *Light Sci. Appl.* **10**, 156 (2021).
30. Grillot, F. et al. Physics and applications of quantum dot lasers for silicon photonics. *Nanophotonics* **9**, 1271–1286 (2020).
31. Galiev, R. R., Kondratiev, N. M., Lobanov, V. E., Matsko, A. B. & Bilenko, I. A. Optimization of laser stabilization via self-injection locking to a whispering-gallery-mode microresonator. *Phys. Rev. Appl.* **14**, 014036 (2020).
32. Tran, M. A., Huang, D. & Bowers, J. E. Tutorial on narrow linewidth tunable semiconductor lasers using Si/III-V heterogeneous integration. *APL Photonics* **4**, 111101 (2019).
33. Morton, P. A. et al. Integrated coherent tunable laser (ICTL) with ultra-wideband wavelength tuning and sub-100 Hz Lorentzian linewidth. *J. Lightwave Technol.* **40**, 1802–1809 (2021).
34. Maier, P. et al. Sub-kHz-linewidth external-cavity laser (ECL) with Si_3N_4 resonator used as a tunable pump for a Kerr frequency comb. *J. Lightwave Technol.* **41**, 3479–3490 (2023).
35. Duan, J. et al. Narrow spectral linewidth in InAs/InP quantum dot distributed feedback lasers. *Appl. Phys. Lett.* **112**, 121102 (2018).
36. Zhao, S. & Grillot, F. Effect of Shockley-Read-Hall recombination on the static and dynamical characteristics of epitaxial quantum-dot lasers on silicon. *Phys. Rev. A* **103**, 063521 (2021).
37. Duan, J. et al. 1.3- μm reflection insensitive InAs/GaAs quantum dot lasers directly grown on silicon. *IEEE Photonics Technol. Lett.* **31**, 345–348 (2019).
38. Xiang, C. et al. 3D integration enables ultralow-noise isolator-free lasers in silicon photonics. *Nature* **620**, 78–85 (2023).
39. Xiang, C. et al. Laser soliton microcombs heterogeneously integrated on silicon. *Science* **373**, 99–103 (2021).
40. Zhang, Z. et al. Photonic integration platform for rubidium sensors and beyond. *Optica* **10**, 752–753 (2023).
41. Zhang, M., Wang, C., Cheng, R., Shams-Ansari, A. & Lončar, M. Monolithic ultra-high-Q lithium niobate microring resonator. *Optica* **4**, 1536–1537 (2017).
42. Snigirev, V. et al. Ultrafast tunable lasers using lithium niobate integrated photonics. *Nature* **615**, 411–417 (2023).
43. Wang, Y. et al. InAs/GaAs quantum-dot lasers grown on on-axis Si (001) without dislocation filter layers. *Opt. Express* **31**, 4862–4872 (2023).
44. Wu, L. et al. Greater than one billion Q factor for on-chip microresonators. *Opt. Lett.* **45**, 5129–5131 (2020).
45. Liu, K. et al. Ultralow 0.034 dB/m loss wafer-scale integrated photonics realizing 720 million Q and 380 μW threshold Brillouin lasing. *Opt. Lett.* **47**, 1855–1858 (2022).
46. Chow, W. W., Wan, Y., Bowers, J. E. & Grillot, F. Analysis of the spontaneous emission limited linewidth of an integrated III–V/SiN laser. *Laser Photonics Rev.* **16**, 2100620 (2022).

47. Alkhazraji, E., Chow, W. W., Grillot, F., Bowers, J. E. & Wan, Y. Linewidth narrowing in self-injection-locked on-chip lasers. *Light Sci. Appl.* **12**, 162 (2023).
48. Fan, Y. et al. Hybrid integrated InP-Si₃N₄ diode laser with a 40-Hz intrinsic linewidth. *Opt. Express* **28**, 21713–21728 (2020).
49. Xiang, C. et al. High-performance lasers for fully integrated silicon nitride photonics. *Nat. Commun.* **12**, 6650 (2021).
50. Larson, M. et al. Narrow linewidth sampled-grating distributed bragg reflector laser with enhanced side-mode suppression. In *Optical Fiber Communication Conference M2D.1* (Optica Publishing Group, 2015).

Publisher's note Springer Nature remains neutral with regard to jurisdictional claims in published maps and institutional affiliations.

Open Access This article is licensed under a Creative Commons Attribution 4.0 International License, which permits use, sharing, adaptation, distribution and reproduction in any medium or format, as long as you give appropriate credit to the original author(s) and the source, provide a link to the Creative Commons licence, and indicate if changes were made. The images or other third party material in this article are included in the article's Creative Commons licence, unless indicated otherwise in a credit line to the material. If material is not included in the article's Creative Commons licence and your intended use is not permitted by statutory regulation or exceeds the permitted use, you will need to obtain permission directly from the copyright holder. To view a copy of this licence, visit <http://creativecommons.org/licenses/by/4.0/>.

© The Author(s) 2024

Methods

Free-running laser characterizations

The optical spectra are measured using a high-resolution optical spectrum analyser (Yokogawa AQ6370C). The laser frequency noise and resultant fundamental linewidth are taken from a commercial laser phase-noise analyser (PNA) (OEWaves OE4000) that internally performs averaging over the measured phase noise. As automated equipment, this PNA offers a measurement bandwidth of 150 MHz. An average of 50 was applied in the range of 1 kHz to 150 MHz to measure the frequency noise. In the measurements of optical spectra, the QD laser is driven by a programmable current source (Keithley 2400). It is then driven by a low-noise laser current source (ILX Lightwave LDX-3620) to ensure stable and low-noise operation in the measurement of frequency noise. The laser RIN is measured by a 20 GHz photodetector (Agilent 11982A). The converted a.c. signal filtered by a bias-tee is preamplified by a 30 dB radio-frequency amplifier (RF-LAMBDA RLNA00G18GA) before it is sent to an electrical spectrum analyser (ESA) (Rohde & Schwarz FSU50). The resolution bandwidth used in the RIN measurement is 1 MHz. The RIN bandwidth is limited by the radio-frequency amplifier, which is 18 GHz.

Laser ECL

Figure 2a depicts the experimental configurations for laser ECL. The coupled laser emission is sent to a 90/10 fibre beamsplitter, after which 90% of the coupled power will be used for EOF. The feedback loop consists of a polarization controller, a variable optical attenuator and a back-reflector (EXFO OSICS BKR). The external cavity frequency is 6 MHz, which corresponds to a 16.6-m-long optical fibre. The remaining 10% of the laser output is utilized for the characterizations of feedback sensitivity and laser linewidth. After passing through an optical isolator, it is transferred either to a PNA (OEWaves OE4000) for frequency-noise characterization or a delayed self-heterodyne setup to check the electrical-spectrum-based laser coherence.

In this study, the feedback strength is determined by the on-chip reflected power (P_{refl}) and the free-space output power (P_{out}) through the following relationship:

$$\eta_F = \frac{P_{\text{refl}}}{P_{\text{out}}} \quad (1)$$

All the losses from the external cavity should be considered to calculate the reflected power and therefore the feedback strength. After optimizing the setup, the fibre–chip coupling loss is -2.40 dB (round-trip coupling loss is -4.80 dB), the total losses from the 90% beamsplitter, insertion loss of the variable optical attenuator, polarization controller and fibre is -4.81 dB. The maximum on-chip feedback strength that we can achieve is -9.61 dB.

In the ECL operation, the laser is driven with low-noise laser current sources (ILX Lightwave LDX-3620) to ensure stable and low-noise operation. The detection of the locking state is assured by the reduction in the linewidth of the self-heterodyne beat. The self-heterodyne interferometer setup basically consists of a Mach–Zehnder interferometer (made from two 3 dB couplers) with a polarization controller and a short delay line in one of its arms and a fibre-coupled acousto-optic modulator (Gooch & Housego 27 MHz) in the other arm (Fig. 2a). The beat frequency from the self-heterodyne interferometer is detected using a photodetector (Newport 1811) before it is sent to an ESA (Rohde & Schwarz FSWP).

To investigate the turnkey locking stability, we periodically vary the on-chip feedback strength between -61.20 and -9.61 dB. The

periodicity of the feedback strength calibration is 80 s. The resolution bandwidth of the ESA was 10 Hz in this measurement.

Data availability

The data used to produce the plots within this paper are available via figshare at <https://doi.org/10.6084/m9.figshare.25057985> (ref. 51).

References

51. Dong, B. et al. Open data for “Turnkey locking of quantum-dot lasers directly grown on Si”. *figshare* <https://doi.org/10.6084/m9.figshare.25057985> (2024).

Acknowledgements

This work is supported by the Defense Advanced Research Projects Agency (DARPA) MTO GRYPHON (HRO011-22-2-0009) and LUMOS (HRO011-20-2-0044) programs. We acknowledge King Abdullah University of Science and Technology (KAUST) under award nos. RFS-OFP2023-5558, ORA-2022-5314 and ORA-2022-5313, and SDAIA-KAUST Center of Excellence in Data Science and Artificial Intelligence (SDAIA-KAUST AI). W.W.C. acknowledges support from the Sandia National Laboratories, a multimission laboratory managed and operated by National Technology & Engineering Solutions of Sandia, LLC, a wholly owned subsidiary of Honeywell International Inc., for the US Department of Energy’s National Nuclear Security Administration under contract DE-NA0003525. This paper describes objective technical results and analysis. Any subjective views or opinions that might be expressed in the paper do not necessarily represent the views of the US Department of Energy or the United States Government. This work was performed, in part, at the Center for Integrated Nanotechnologies, an Office of Science User Facility operated for the U.S. Department of Energy (DOE) Office of Science.

Author contributions

B.D. and Y.W. led the QD laser design and device characterization. Y.W. designed and fabricated the QD lasers with assistance from C.S. and R.K. B.D. characterized and gathered the experimental data from the device, with contributions from R.K. W.W.C. provided the theoretical calculations and analysis on the locking dynamics and feedback sensitivity, with contributions from A.P., E.A. and H.W. B.D. wrote the paper with inputs from Y.W., C.S., E.A. and A.P. All authors commented on and edited the paper. J.E.B. supervised the project.

Competing interests

J.E.B. is a co-founder and shareholder of Nexus Photonics and Quintessent—startups in silicon photonics. The other authors declare no competing interests.

Additional information

Supplementary information The online version contains supplementary material available at <https://doi.org/10.1038/s41566-024-01413-2>.

Correspondence and requests for materials should be addressed to Yating Wan or John E. Bowers.

Peer review information *Nature Photonics* thanks the anonymous reviewer(s) for their contribution to the peer review of this work.

Reprints and permissions information is available at www.nature.com/reprints.